# Assessment of the Microstructure, Solidification Characteristics and Mechanical Properties of AZ61 + *x*Sr Magnesium Alloys

F. YAVARI and S.G. SHABESTARI

The effect of Sr addition on the solidification parameters of AZ61 alloy, such as liquidus and solidus temperatures, the nucleation under cooling temperature and dendrite coherency point (DCP), was investigated *via* the cooling curve thermal analysis method. The results revealed that by increasing the Sr content from 0 to 0.75 pct, the nucleation temperature increased about 8.2 °C and nucleation under cooling decreased about 3.5 °C. Also, it was found that increasing the Sr content suspended the dendrite coherency point and increased the solid fraction at this point. Mechanical properties of AZ61 alloy were characterized at room temperature through a compressive test. The results indicated the positive influence of Sr on compressive strength of the alloy. When the Sr content increased from 0 to 0.75 pct, the ultimate compressive stress increased from 186 to 280 MPa. This could be the result of a grain refining effect of Sr on AZ61 alloy and the formation of $Al_4Sr$ and $Al_3Mg_{13}Sr$ intermetallic compounds.

https://doi.org/10.1007/s11663-020-01971-0


## I. INTRODUCTION

In recent years, the demand for magnesium alloys has increased in the automotive, aerospace and other industries because of their light weight. In particular, Mg-Al alloys such as AZ (Mg-Al-Zn) and AM (Mg-Al-Mn) series are very attractive because of their superior castability, good balance between strength and ductility and low cost.[1–4] However, mechanical properties of these alloys weaken at elevated temperatures. $\beta$-$Mg_{17}Al_{12}$ phase is recognized as the reason for poor mechanical properties of Mg-Al alloys at elevated temperatures.[5–7] Several studies have been done on these alloys by addition of elements such as RE, Si, Ca and Sr to improve them.[5–9] Strontium has been found to be an effective element in Mg-Al alloys. It can refine the grain size of Mg-Al alloys and improve the mechanical properties of these alloys at room and elevated temperatures.[3,4,7–11] Hirai *et al.*[8] and Ming-bo *et al.*[11] studied the effect of Sr on the grain size of AZ91 and AZ31 alloys respectively in different works. Their studies revealed that Sr can considerably decrease the grain size in AZ91 and AZ31 alloys. Zeng *et al.*[3] reported that Sr addition to AZ31 in addition to grain refining can improve the tensile properties at room temperature (yield strength and elongation). Zhao *et al.*[9] studied the effect of Sr on the mechanical properties of AM50 at elevated temperatures and reported that Sr improves the tensile properties and creep resistance of this alloy. They claimed that the formation of a thermally stable $Al_4Sr$ intermetallic compound, which also caused the reduction of $\beta$-$Mg_{17}Al_{12}$ phase, is the main reason for the improvement of the mechanical properties of AM50 at elevated temperatures.

However, there is no report on the influence of Sr addition on the solidification characteristics of Mg-Al alloys such as the nucleation and growth temperatures, range of solidification temperature, temperature of eutectic reactions and so on. Understanding of these parameters could help to predict the microstructure and mechanical behavior of the alloys. The aim of this article is to determine how different amounts of Sr affect the solidification parameters of AZ61 magnesium alloy. To achieve this goal, the cooling curve thermal analysis (CCTA) method was used. Also, the microstructure and compressive strength of samples were studied.

## II. EXPERIMENTAL PROCEDURES

### A. *Material*

Samples were prepared by melting high-purity magnesium ingots in a cylindrical stainless steel crucible in an electrical resistance furnace. Then, the appropriate amounts of pure aluminum and zinc and Al-10Sr master alloy were added into the melt at 700 °C, and it was

F. YAVARI and S.G. SHABESTARI are with the School of Metallurgy and Materials Engineering, Iran University of Science and Technology (IUST), 16846-13114, Narmak, Tehran, Iran Contact e-mail: shabestari@iust.ac.ir

Manuscript submitted April 1, 2020.
Article published online September 28, 2020.

mechanically stirred for 2 minutes by a steel rod. The melt was held for 10 minutes at 700 °C in the furnace for homogenizing before being poured into a preheated steel mold. The samples were cooled at room temperature without any isolation. All the melting processes were done under protection of anti-oxidizing flux and inert argon gas atmosphere from oxidation. The chemical composition of samples is given in Table I.

### B. *Thermal Analysis*

Cooling curve thermal analysis was conducted by re-melting and pouring of approximately 150 g of each sample into a simple thin-walled stainless steel cup (outer diameter 40 mm, height 70 mm and wall thickness 1 mm) at the temperature of 700 °C. Two K-type thermocouples (chromel-alumel) were located on it, one in the center and another near the wall of the cup, both at a position 20 mm from the bottom. The experimental setup for the thermal analysis and location of thermocouples is schematically shown in Figure 1. The thermocouples were shielded by a stainless steel sheath and linked to a high-speed data acquisition system (A/D converter) connected to a notebook computer. The ADAM-4018 analog to digital converter used in this study has a sensitive 16-bit microprocessor-controlled sigma-delta A/D converter, response time of 0.02 second and an eight-channel analog input module that provides programmable input ranges on all channels. Thermocouples were calibrated using a high-purity aluminum melt before the tests were done. To certify the accuracy and reliability of the results, each test was carried out at least three times. The cooling rate during thermal analysis tests was 0.55 ± 0.05 °C/s, which was calculated from the slope of the cooling curve, $\Delta T/\Delta t$, at the temperature interval in the mushy zone between the liquidus point and first eutectic reaction (610 °C to 585 °C).

### C. *Microstructural Evaluation*

Thermal analysis samples were sectioned horizontally through the area close to where the tip of the thermocouples was located. After grinding and polishing the samples, they were etched using 3 pct Nital (3 ml nitric acid + 100 ml ethanol) and acetic-picric acid (30 ml acetic acid + 15 ml $H_2O$ + 6 g picric acid + 100 ml ethanol) to reveal the micro- and macrostructure, respectively. The grain structures were observed using a HUVITZ-HM25-type optical microscope. For each sample, five pictures were taken from the central zone, and the grain size was evaluated for every picture based on the linear intercept method described in ASTM standard E112-88. Then, the average grain size of each sample was calculated. BSE micrographs, EDS and X-ray mapping analyses for microstructural evaluations were taken using the Tescan-Vega II scanning electron microscopy (SEM). The chemical composition of intermetallic phases was determined using energy-dispersive X-ray analysis linked to SEM.

**Table I. Chemical Compositions of the Investigated Alloys**

| | Elements/Mass Pct | | | |
|---|---|---|---|---|
| Nominal Alloys | Al | Zn | Sr | Mg |
| AZ61 | 6.42 | 1.14 | 0 | balance |
| AZ61 + 0.1Sr | 6.38 | 1.07 | 0.12 | balance |
| AZ61 + 0.25Sr | 6.29 | 1.08 | 0.23 | balance |
| AZ61 + 0.5Sr | 6.31 | 1.12 | 0.53 | balance |
| AZ61 + 0.75Sr | 6.40 | 1.02 | 0.72 | balance |

### D. *Mechanical Tests*

Mechanical properties were characterized by the compressive test at room temperature. Compressive test specimens were prepared by casting into a cylindrical steel mold, and then, they were machined. Final samples had a gauge length of 15 mm and diameter of 10 mm. Compressive mechanical tests were performed using an INSTRON 8562 machine at a deformation rate of 1 mm/min. Both ends of the specimens were polished to make them parallel to each other prior to the compression test. Each alloy was tested three times to assure reliability of the results.

## III. RESULTS AND DISCUSSION

### A. *Microstructural Evaluation*

The microstructure of the AZ61 sample contains two main phases: α-Mg matrix and β-$Mg_{17}Al_{12}$, which are shown as phases A and B in Figure 2(a). Figure 2(b) shows that addition of Sr formed new phases. Based on

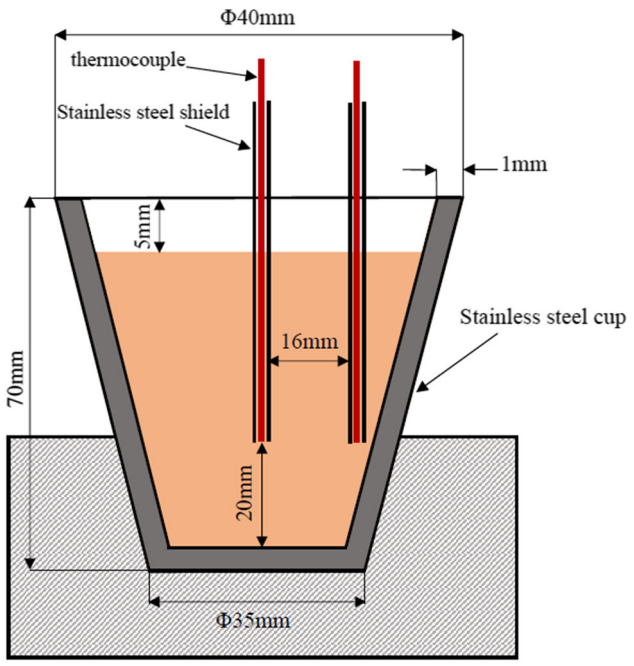


Fig. 1—Schematic of the experimental setup for the thermal analysis and location of thermocouples.

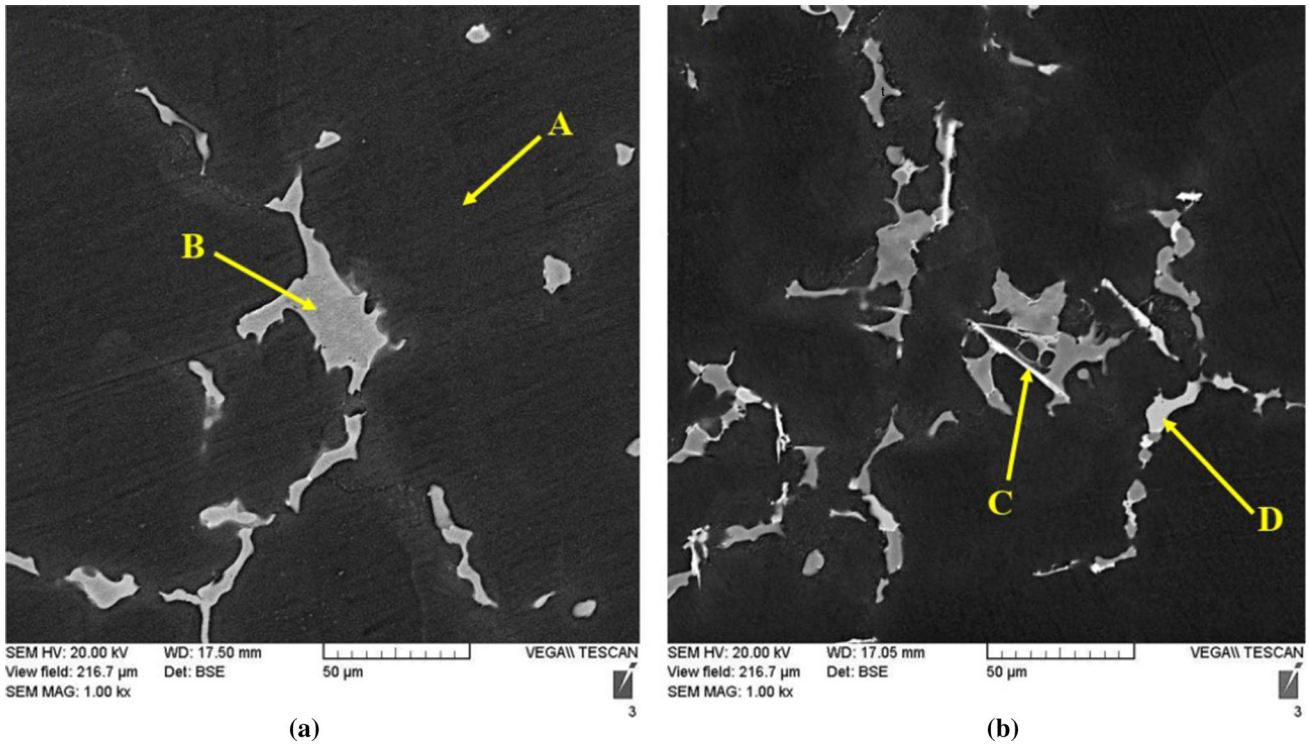


Fig. 2—SEM micrograph of (*a*) AZ61 and (*b*) AZ61 + 0.5Sr alloys.

**Table II. EDS Analysis Results of the Phases Indicated in Fig. 1**

| | Elements/Atom Pct | | | | |
|---|---|---|---|---|---|
| Point | Mg | Al | Zn | Sr | Phase |
| A | 96.90 | 2.17 | 0.93 | — | α-Mg |
| B | 65.06 | 34.45 | — | — | $\beta$-$Mg_{17}Al_{12}$ |
| C | 64.47 | 28.06 | — | 7.47 | $Al_4Sr$ |
| D | 74.84 | 19.33 | — | 5.83 | $Al_3Mg_{13}Sr$ |

the EDS analysis results provided in Table II, the first phase, which is characterized as a needle-like morphology (phase C in Figure 2), contains 64.47 at. pct Mg, 28.06 at. pct Al and 7.47 at. pct Sr. Therefore, this phase corresponds to $Al_4Sr$.[2,3,7,12] The measured content of Mg in this phase is caused by its small dimensions and the influence of α-Mg phase of the matrix on the EDS analysis. The second component appears as slightly brighter than $\beta$-$Mg_{17}Al_{12}$ and darker than $Al_4Sr$ (phase D in Figure 2). Concentrations of Mg, Al and Sr in this phase are 74.84 at. pct, 19.33 at. pct and 5.83 at. pct, respectively. This ternary intermetallic compound has been reported as $Al_3Mg_{13}Sr$ in the Mg-Al-Sr alloys.[3, 7, 12] $Al_3Mg_{13}Sr$ appeared in samples having strontium > 0.25 pct Sr. X-ray mapping analyses of these two compounds, C and D, are illustrated in Figures 3 and 4, respectively. Figure 3 indicates that phase C is needle-like and contains Al and Sr atoms. The best stoichiometry for this intermetallic is $Al_4Sr$. It also indicates that $\beta$-$Mg_{17}Al_{12}$ has nucleated on this phase. This means that $Al_4Sr$ phase formed before $\beta$-$Mg_{17}Al_{12}$. The results of thermal analysis also confirmed this statement. Figure 4 shows phase D, which contains Al, Mg and Sr atoms. The best stoichiometry for this intermetallic is $Al_3Mg_{13}Sr$.

Figure 5 indicates the effect of Sr addition on the macrostructure of AZ61 alloy. This figure reveals that by increasing the Sr content the grain size decreases significantly in AZ61 alloy. Effect of Sr content on the grain size of AZ61 is indicated in Figure 6. According to this figure, by increasing the Sr content up to 0.75 pct, the grain size was decreased from 190 $\mu$m to 100 $\mu$m. Other researchers have also reported that strontium can refine the grains in Mg-Al alloys.[3,4,8,10,13] None of the intermetallic components that formed in AZ61 + Sr samples can act as the heterogeneous nucleation for α-Mg grains. Researchers have suggested that the mechanism of grain refinement is the GRF (growth restriction factor) mechanism.[3,10,13]

$$\mathrm{GRF} = \sum_i m_i C_{0i}(k_i - 1)$$

where $m_i$ is the slope of the liquidus line, $k_i$ is the partition coefficient, and $C_{0i}$ is the initial concentration of element i.

The solid solubility of Sr solute in magnesium is relatively limited, and thus rapid enrichment of Sr in the liquid ahead of the growing interface will restrict the grain growth during solidification. As a result, the grain size of AZ61 alloy decreases with Sr addition.

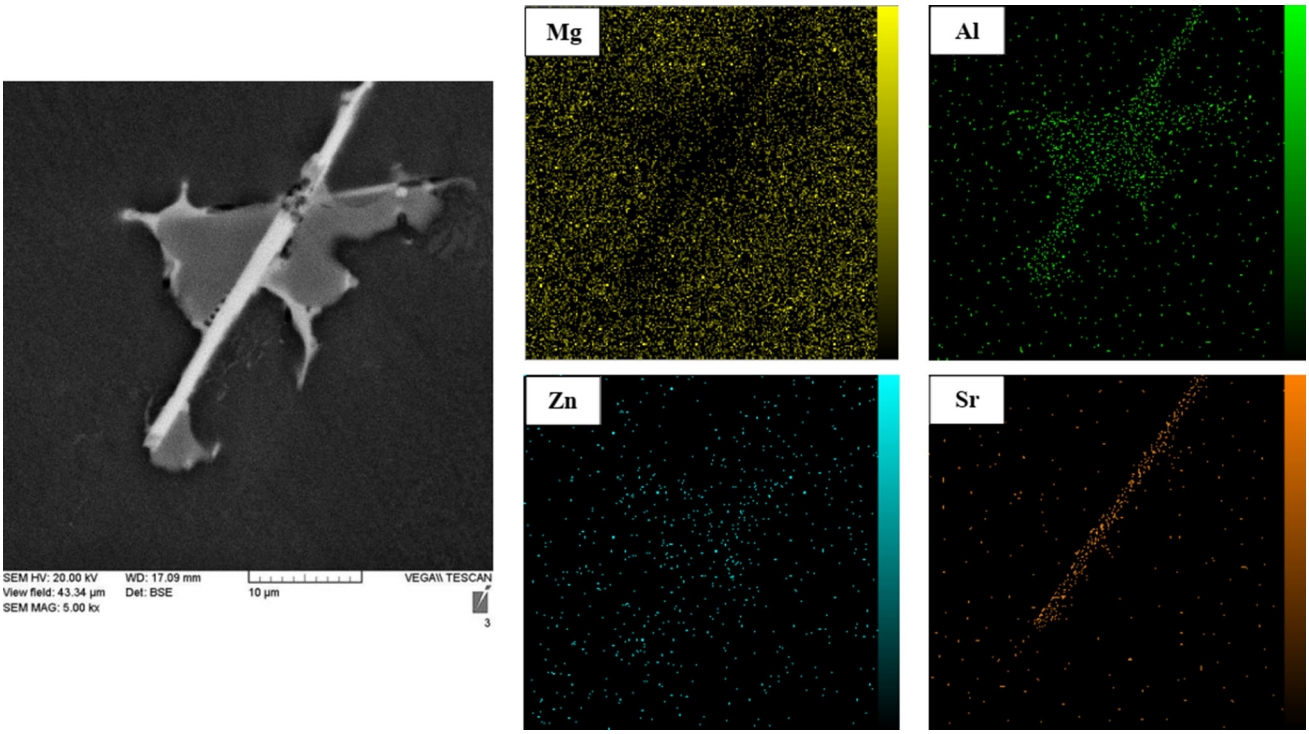


Fig. 3—X-ray mapping analyses of $Al_4Sr$ intermetallic compound.

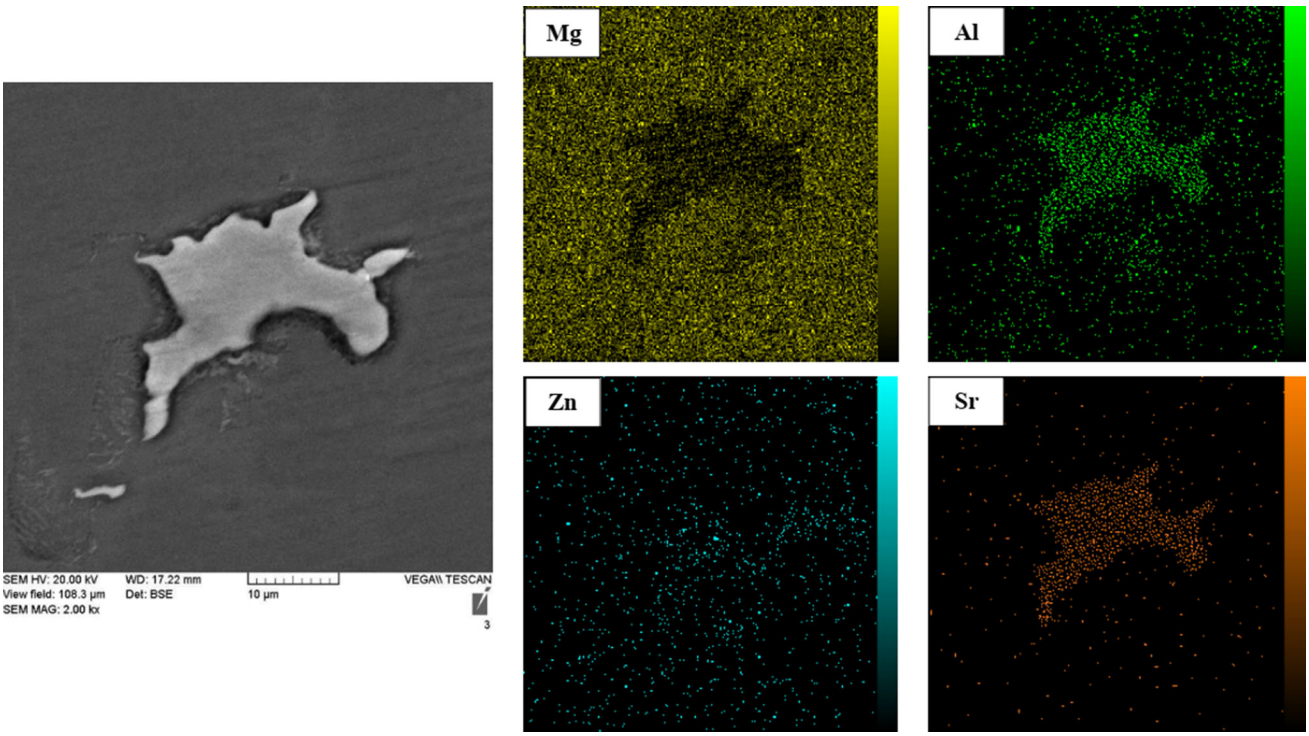


Fig. 4—X-ray mapping analyses of $Al_3Mg_{13}Sr$ intermetallic compound.

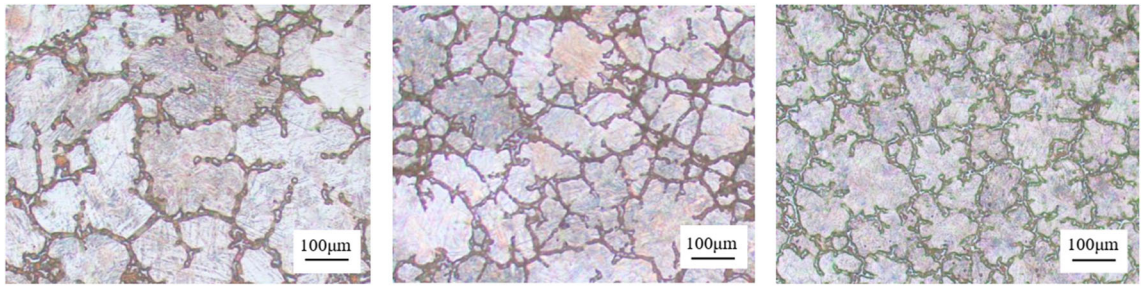


Fig. 5—Grain refining effect of Sr on AZ61 alloy.

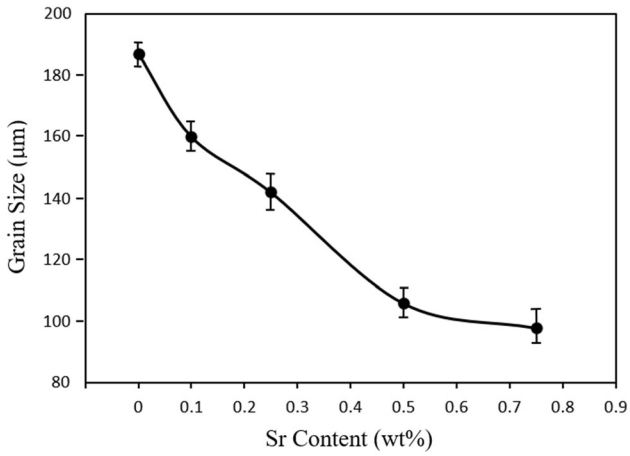


Fig. 6—Effect of Sr content on the grain size of AZ61 alloy.

## B. *Thermal Analysis*

The cooling curves recorded for AZ61 and AZ61 + 0.5Sr and their first and second derivative curves are exhibited in Figure 7. There are two distinct peaks on the first derivative curve of AZ61. The first peak at 627 °C and the last one at 425 °C are representative of the formation of α-Mg matrix and $\beta$-$Mg_{17}Al_{12}$ phase in the eutectic reaction, respectively. Two other peaks, which appeared by addition of 0.5 pct strontium at 578 °C and 557 °C, relate to the formation of $Al_4Sr$ and $Al_3Mg_{13}Sr$ intermetallic compounds based on the microstructural evaluation. $Al_3Mg_{13}Sr$ appeared in the microstructure only after addition of 0.5 pct Sr. Therefore, the third peak in the thermal analysis result of the sample with 0.25 pct Sr at 580 °C is considered formation of $Al_4Sr$ since there is no other phase in the microstructure. Therefore, it is concluded that the fourth peak in the thermal analysis result of the sample with 0.5 pct Sr at 557 °C relates to the formation of $Al_3Mg_{13}Sr$. Probable transformations occurring during solidification of AZ61 + $x$Sr are summarized in Table III.

### 1. *Liquidus parameters*

Solidification parameters including nucleation, growth and minimum temperatures ($T_N$, $T_G$ and $T_{min}$) for all reactions, nucleation undercooling of α-Mg ($\Delta T_{N,\alpha} = T_{N,\alpha} - T_{min,\alpha}$), solidus temperature ($T_S$) and solidification range ($\Delta T_S = T_{N,\alpha} - T_S$) for all the alloys are extracted from cooling curves and their derivations based on the previous studies.[14–19] Figure 8 indicates how characteristic temperatures of a reaction during solidification can be determined from the cooling curve and its first derivation. When the solidification process starts by nucleation of primary dendrites, a detectable peak related to the start of solidification appears in both the first and second derivative curves. The nucleation temperature is the minimum point just before the perceptible peak, which is related to the starting point of solidification. Increasing the amount of both second and first derivative curves at the start point of solidification is related to the amount of latent heat released during the formation of the first solid phase nuclei in molten metal. It is the same for any other reactions during the solidification.[14] Solidification parameters for AZ61 + $x$Sr alloys are extracted and summarized in Table IV.

The thermal analysis result reveals that by increasing the amount of strontium up to 0.75 pct, the nucleation temperature of AZ61 alloy increases from 627.5 °C to 635.7 °C and the nucleation undercooling temperature ($\Delta T_{N,\alpha} = T_{N,\alpha} - T_{min,\alpha}$) decreases slightly from 10.3 to 6.8. Backerud *et al.*[15] and Shabestari *et al.*[17,19] reported that the grain refining process affects the cooling curve of the alloy, in which it increases the nucleation temperature and decreases the nucleation undercooling temperature. As the grain refiner increases the nucleation sites present in the melt, nucleation can occur at higher temperatures and needs a lower driving force of nucleation undercooling. Therefore, the thermal analysis results presented in Table IV and macrostructural evaluation indicated in Figure 6 confirm the grain refining effect of Sr on AZ61 alloy.

### 2. *Solidus parameters*

Based on the results presented in Table IV, the temperature of the final eutectic reaction (formation of $\beta$-$Mg_{17}Al_{12}$) was decreased considerably by increasing the amount of strontium. The start of the final eutectic reaction (reaction number 4 in Table III) decreased from 428.8 °C to 414.6 °C by increasing the amount of strontium from zero to 0.75 pct Sr. This means that the nucleation temperature of the final eutectic reaction decreased by about 14.2 °C. Since the formation of $Al_4Sr$ and $Al_3Mg_{13}Sr$ intermetallic compounds consumes Al in the molten alloy, the melt reaches to the

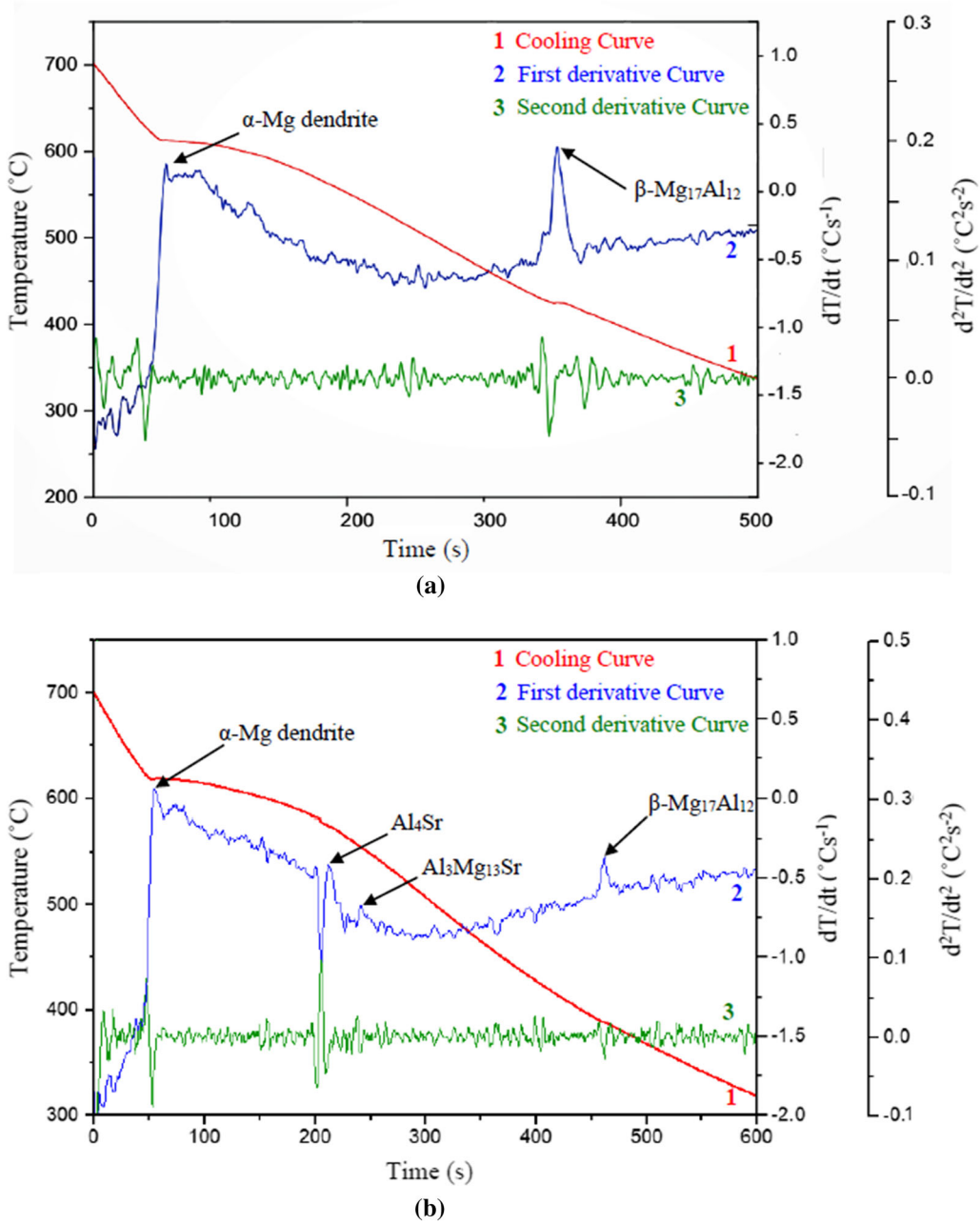


Fig. 7—Cooling curve and its first and second derivative curves (*a*) AZ61 and (*b*) AZ61 + 0.5Sr.

**Table III. Probable Transformations Occurring During Solidification of AZ61 + *x*Sr Alloys Indicated in Fig. 5**

| No. | Chemical Reactions |
|---|---|
| 1 | nucleation of α-Mg |
| 2 | $L \rightarrow \alpha\text{-Mg} + Al_4Sr$ |
| 3 | $L \rightarrow \alpha\text{-Mg} + Al_3Mg_{13}Sr$ |
| 4 | $L \rightarrow \alpha\text{-Mg} + \beta\text{-}Mg_{17}Al_{12}$ |

eutectic composition later. Therefore, the formation of these phases probably postponed the final eutectic reaction.

In the literature,[14–16] the finishing point of solidification is obtained from the first minimum point after the last sensible peak related to the end of solidification in the first derivative curve. The solidus temperature of AZ61 magnesium alloy was decreased from 422 °C to 409.1 °C by increasing the Sr content up to 0.75 pct. As

a result of the increase in nucleation temperature of α-Mg and decrease in the finishing point of solidification, the solidification range ($\Delta T_S$) is increased from 205.5 °C to 226.6 °C by increasing the Sr content up to 0.75 pct.

3. *Dendrite coherency point (DCP)*

The dendrite coherency point (DCP) is defined as the point during solidification where the dendrite tips begin to impinge on one another with continuous growth and the dendritic network becomes coherent. This is a critical stage during solidification because at this point mass feeding passes to inter-dendritic feeding and casting defects start after dendrite coherency has occurred. This point is determined by two factors: the dendrite coherency temperature ($T_{DCP}$) and dendrite coherency solid fraction ($f_{DCP}$). In this investigation, the two thermocouple cooling

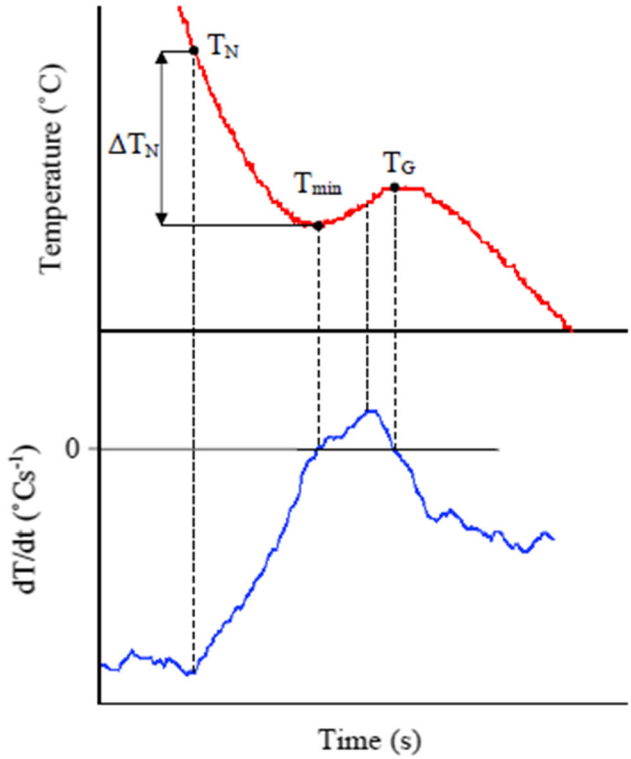


Fig. 8—Characteristic temperatures of a reaction during solidification from the cooling curve and its first derivation.

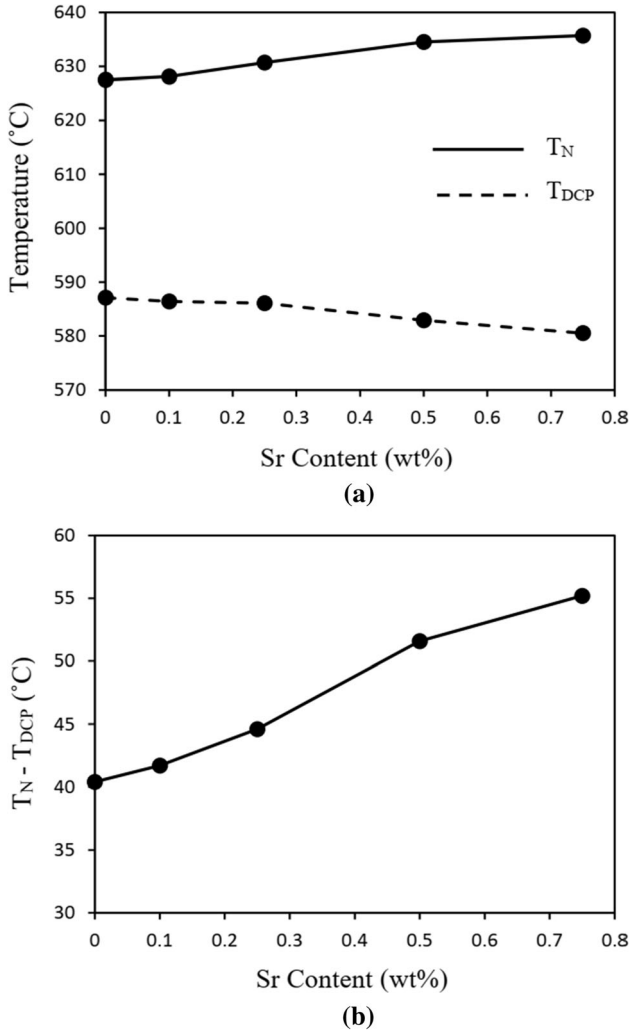


Fig. 9—Effect of Sr content on (*a*) nucleation and coherency temperatures, (*b*) the temperature range between the nucleation and coherency of AZ61 alloy.

**Table IV. Solidification Parameters of AZ61 + *x*Sr Alloys**

| | α-Mg Dendrites | | | | $Al_4Sr$* | | $Al_3Mg_{13}Sr$** | | $\beta$-$Mg_{17}Al_{12}$ in Eutectic | | | |
|---|---|---|---|---|---|---|---|---|---|---|---|---|
| Sr Pct | $T_N$ | $T_G$ | $T_{min}$ | $\Delta T_N$ | $T_N$ | $T_G$ | $T_N$ | $T_G$ | $T_N$ | $T_G$ | $T_S$ | $\Delta T_S$ |
| 0 | 627.5 | 618.6 | 617.2 | 10.3 | — | — | — | — | 428.8 | 424.2 | 422.0 | 205.5 |
| 0.1 | 628.1 | 619.4 | 618.0 | 10.1 | — | — | — | — | 426.5 | 423.3 | 420.2 | 207.9 |
| 0.25 | 630.7 | 622.8 | 621.9 | 8.8 | 580.1 | 578.6 | — | — | 418.6 | 414.4 | 411.6 | 219.1 |
| 0.5 | 634.5 | 627.8 | 627.4 | 7.1 | 578.2 | 574.8 | 557.3 | 555.5 | 415.3 | 412.1 | 409.5 | 225.0 |
| 0.75 | 635.7 | 629.2 | 628.9 | 6.8 | 5.78.7 | 475.2 | 558.6 | 555.8 | 414.6 | 410.9 | 409.1 | 226.6 |

*Because of the small amount of $Al_4Sr$ intermetallic compound in AZ61 + 0.1Sr, the latent heat of the reaction is not enough and its peak is not recognizable.

**This compound did not appear in samples having Sr < 0.5 pct.

curve thermal analysis technique is used to detect DCP. This technique has been explained comprehensively in previous research.[20,21] The dendrite coherency temperature and solid fraction at this point for AZ61 + $x$Sr alloys were extracted from thermal analysis curves.

Figure 9 shows the effect of Sr content on the dendrite coherency temperature and temperature range between the nucleation temperature and DCP ($T_N - T_{DCP}$). $T_N - T_{DCP}$ is more important than the individual temperature of $T_{DCP}$ because the nucleation temperature is not constant when the Sr amount increases. This temperature range corresponds to the free dendritic growth stage during solidification.[20] When the Sr amount increases to 0.75 pct, the temperature difference between the nucleation of α-Mg and coherency of dendrites rises from 40.4 °C to 55.2 °C. In other words, the coherency point is postponed by adding strontium to the AZ61 alloy.

Solid fraction curves are calculated based on the Newtonian model adopted by Stefanescu *et al.* and Tamminen 22, and the solid fractions at DCP are obtained for all samples. The influence of the Sr content on the coherency solid fraction is shown in Figure 10. According to this figure, increasing the Sr content up to 0.75 pct causes a significant increase in the coherency solid fraction in which it increases from 19.2 to 27.9 pct.

It has been mentioned that Sr addition decreases the grain size of AZ61 alloy by the GRF mechanism. In other words, the grain refining effect of Sr causes a decelerated growth rate of α-Mg dendrites. As a result, α-Mg dendrites become coherent later and the temperature difference between nucleation and coherency increases by increasing the Sr content. Since increasing the Sr content causes a diminishing growth rate of dendrites and increases the temperature range between nucleation and coherency, inter-dendritic feeding is postponed and the amount of solid phase before dendrite coherency is increased.

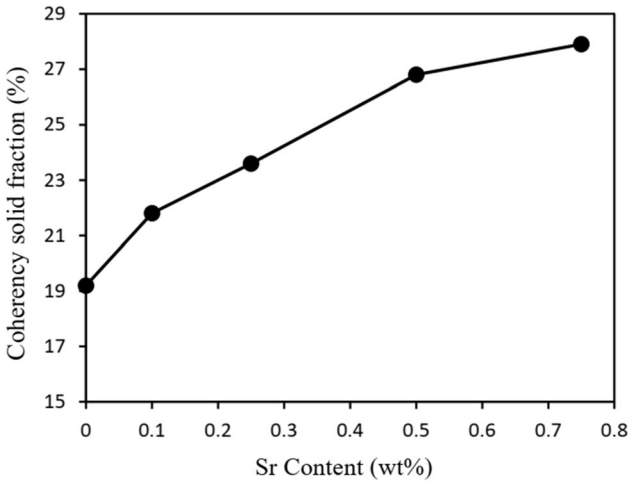


Fig. 10—Effect of Sr content on the dendrite coherency solid fraction of AZ61 alloy.

## C. *Mechanical Properties*

The results of room temperature compressive tests are given in Figure 11, which shows that Sr can improve the compressive strength of AZ61 alloy. By increasing the Sr content up to 0.75 pct, the yield stress increases from 112 to 196 MPa and compressive stress increases from 170 to 325 MPa. There can be two reasons for improving the compressive strength of AZ61 by adding strontium:

1. Based on the Hall-Petch theory, the refining effect of Sr addition causes strengthening of AZ61 alloy.[3,8]
2. The formation and distribution of Sr containing intermetallic compounds such as $Al_4Sr$ and

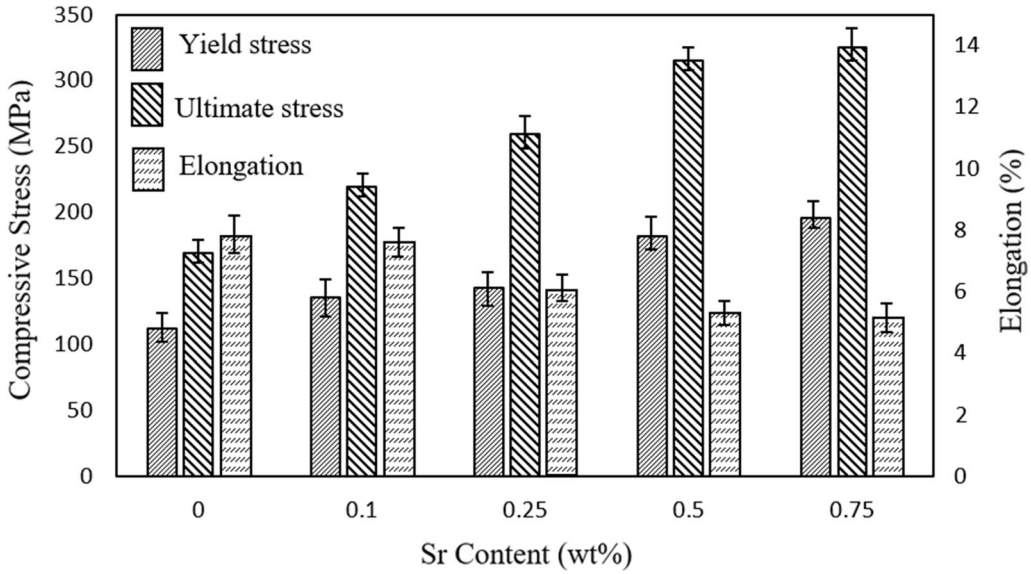


Fig. 11—Effect of Sr content on room temperature compressive strength and elongation of AZ61 alloy.

$Al_3Mg_{13}Sr$, which are hard phases, can increase the strength of AZ61 alloy.

On the other hand, formation of intermetallic compounds caused the reduction of elongation. According to Figure 11, by adding 0.75 pct Sr, elongation of AZ61 decreases from 7.8 to 5.1 pct. Therefore, Sr addition can improve the strength of AZ61 alloy while weakening its ductility.

## IV. CONCLUSIONS

The effect of Sr addition on the solidification parameters of AZ61 magnesium alloy was comprehensively investigated. Also, the effect of Sr on the microstructure and compressive strength of AZ61 alloy was studied. The results of this investigation can be summarized as follows:

1. By adding 0.1 pct Sr to AZ61alloy, an $Al_4Sr$ intermetallic compound with needle-like morphology appears in the microstructure. Also, in alloys having strontium $>$ 0.25 pct Sr, a ternary intermetallic compound identified as $Al_3Mg_{13}Sr$ is found in the alloy.
2. Strontium can act as a grain refiner in AZ61 magnesium alloy. The grain refinement is based on the GRF mechanism.
3. By adding strontium to AZ61 alloy, two well-defined peaks appear in the first derivative cooling curve at 578 °C and 557 °C, which relate to the formation of $Al_4Sr$ and $Al_3Mg_{13}Sr$, respectively.
4. The nucleation temperature of AZ61 alloy increases from 627.5 °C to 635.7 °C and the nucleation undercooling temperature decreases from 10.3 to 6.8 by increasing the amount of strontium up to 0.75 pct.
5. The final eutectic reaction is postponed by adding strontium to AZ61alloy. The solidus temperature of AZ61 alloy decreases by about 12.9 °C as a result of increasing Sr content up to 0.75 pct.
6. Addition of Sr postpones dendrite coherency and forms more solid phase before coherency occurrence. Therefore, by increasing the Sr content up to 0.75 pct, the temperature range between the nucleation of α-Mg and coherency of dendrites increases from 40.4 °C to 55.2 °C and the coherency solid fraction increases from 19.2 to 27.9 pct.
7. Sr addition has a positive effect on the compressive strength of AZ61 alloy as a result of grain refinement and formation of Sr containing intermetallic compounds, but it reduces the ductility.

## REFERENCES


1. G.L. Esperance, P. Plamondon, M. Kunst, and A. Fischersworring-Bunk: *Intermetallics*, 2010, vol. 18, pp. 1–7.
2. J. Bai, Y. Sun, F. Xue, S. Xue, J. Qiang, and T. Zhu: *J. Alloys Compds.*, 2007, vol. 437, pp. 247–53.
3. X. Zeng, Y. Wang, W. Ding, A.A. Luo, and A.K. Sachdev: *Metall. Mater. Trans. A*, 2006, vol. 37A, pp. 1333–41.
4. J. Du, J. Yang, M. Kuwabara, W. Li, and J. Peng: *J. Alloys Compds.*, 2009, vol. 470, pp. 228–32.
5. F. Khomamizadeh, B. Nami, and S. Khoshkhooei: *Metall. Mater. Trans. A*, 2005, vol. 36A, pp. 3489–94.
6. E. Mohammadi Mazraeshahi, B. Nami, S.M. Miresmaeili, and S.M. Tabatabaei: *Mater. Des.*, 2015, vol. 76, pp. 64–70.
7. J. Kubásek, D. Vojtěch, and M. Martínek: *Mater. Charact.*, 2013, vol. 86, pp. 270–82.
8. K. Hirai, H. Somekawa, Y. Takigawa, and K. Higashi: *Mater. Sci. Eng. A*, 2005, vol. 403, pp. 276–80.
9. P. Zhao, Q. Wang, C. Zhai, and Y. Zhu: *Mater. Sci. Eng. A*, 2007, vol. 444, pp. 318–26.
10. S.F. Liu, B. Li, X.H. Wang, W. Su, and H. Han: *J. Mater. Process. Technol.*, 2009, vol. 209, pp. 3999–4004.
11. Y. Ming-bo, P. Fu-Sheng, C.H. Ren-Ju, and T. Ai-Tao: *Trans. Nonferrous Met. Soc. China*, 2008, vol. 18, pp. 52–58.
12. M. Aljarraha, M.A. Parveza, J. Lib, E. Essadiqib, and M. Medraj: *Sci. Technol. Adv. Mater.*, 2007, vol. 8, pp. 237–48.
13. R. Chenga, F. Pana, S. Jianga, C. Lia, B. Jianga, and X. Jiang: *Prog. Nat. Sci.: Mater. Int.*, 2013, vol. 23, pp. 7–12.
14. F. Yavari and S.G. Shabestari: *J. Thermal Anal. Calorim.*, 2017, vol. 129, pp. 655–62.
15. L. Backerud, G. Chai and J. Tamminen, Solidification characteristics of aluminum alloys, Vol. 2: Foundry Alloys, Skanauminum, Stockholm-Sweden, 1990.
16. M.H. Ghoncheh, S.G. Shabestari, and M.H. Abbasi: *J. Thermal Anal. Calorim.*, 2014, vol. 117, pp. 1253–61.
17. S.G. Shabestari and M. Malekan: *J. Alloys Compd.*, 2010, vol. 492, pp. 134–42.
18. J. Li, R. Chen, Y. Ma, and W. Ke: *Thermochim. Acta*, 2014, vol. 590, pp. 232–41.
19. O. Sedighi, S.G. Shabestari, and F. Yavari: *Thermochim. Acta*, 2018, vol. 667, pp. 165–72.
20. M. Malekan and S.G. Shabestari: *Metall. Mater. Trans. A*, 2009, vol. 40A, pp. 3196–3203.
21. M.H. Ghoncheh and S.G. Shabestari: *Metall. Mater. Trans. A*, 2015, vol. 46A, pp. 1287–99.
22. L. Backerud, E. Krol and J. Tamminen, Solidification Characteristics of Aluminum Alloys, Vol. 1: Wrought Aluminum Alloys, Skan Aluminum, Sweden, 1986.